Three-Dimensionally Confined Modes in Micropost Microcavities: Quality Factors and Purcell Factors

Matthew Pelton, Jelena Vučković, *Member, IEEE*, Glenn S. Solomon, Axel Scherer, and Yoshihisa Yamamoto, *Senior Member, IEEE*

***Abstract*—We present detailed calculations of the mode structure of distributed-Bragg-reflector micropost microcavities. Two methods are used: a first-principles, finite-difference time-domain model, and an approximate, heuristic model based on the separation of variables. We calculate modal quality factors, as well as enhancement of spontaneous emission rates, from single quantum dots in the microcavities. Both ideal and realistic post shapes are considered. The two methods give similar results, and are capable of accurately predicting experimentally measured values.**

***Index Terms*—Cavity quantum electrodynamics, microcavities, photonic bandgaps, quantum dots, spontaneous emission modification.**

I. Introduction

THE rate at which a dipole spontaneously emits radiation can be modified by placing the emitter inside an optical cavity [1], [2]. This phenomenon, known as the Purcell effect, has been verified by numerous experiments that involve atoms passing through cavities [3]–[5]. Innovations in semiconductor technology have made it possible to reproduce these results in the solid state by replacing the atoms with quantum dots. Unlike atoms, the quantum dots have the advantages of being relatively simple to study and of being naturally fixed in location. Furthermore, they are produced using highly developed semiconductor techniques, lending to the potential for device applications.

The Purcell factor describes the amount by which the spontaneous emission rate is enhanced for an emitter on resonance with a cavity mode. This factor is proportional to the quality factor Q of the mode and is inversely proportional to the mode volume V_o. Various semiconductor cavities have been investigated to give high Q (*i.e.*, long photon storage time) and tight three-dimensional confinement, including whispering-gallery modes in microdisks [6], defect modes in photonic crystals [7], and micropost microcavities [8]–[10]. Compared to the other cavity geometries, micropost microcavities have several advantages. They can be designed so that light will escape from them normal to the semiconductor sample in a single-lobed Gaussian-like pattern. As well, it is relatively straightforward to isolate single quantum dots in these cavities, allowing for efficient coupling of emission from single dots into single optical modes [11]. The quantum-dot micropost-microcavity system is thus promising for various applications, including high-efficiency light-emitting diodes with broad modulation bandwidth and triggered single-photon sources [12], [13].

Understanding how light from quantum dots couples to these cavities, however, requires a detailed understanding of the cavity mode structure. Similar cavities have been investigated for several years, generally in the context of producing low-threshold lasers [14], [15]. However, distributed emitters were usually considered, not isolated quantum dots, and idealized post geometries were treated. In this paper, we present a detailed study of modes in micropost microcavities with realistic shapes and of coupling from single quantum dots into these modes. A finite-difference time-domain (FDTD) model is presented, which directly gives resonant field distributions, quality factors, and enhancement factors. The results of this model are compared to those of an approximate, heurustic model. Finally, the predictions of the two models are compared quantitatively to experimental results. The models do not involve any fitting parameters, so that they could easily be applied to structures of different shapes and compositions from those considered here.

II. Micropost Microcavities

Fig. 1 is a scanning-electron microscope image of a micropost microcavity of the type considered here. Confinement in the transverse direction (along the post cross-section) is due to total internal reflection at the interface between the high-index semiconductor material and the surrounding air or vacuum. Confinement in the longitudinal direction is provided by a pair of distributed Bragg reflectors (DBRs), or dielectric mirrors. These consist of alternating layers of AlAs and GaAs, each with an optical thickness equal to one-quarter of the chosen cutoff wavelength. The partial reflections from all the interfaces in the DBRs add up in phase, making the overall structure a high reflector within a spectral and angular stopband. The two DBRs are separated by a wavelength-thick spacer layer of GaAs, in which the optical field is trapped. Quantum dots are located in the center of the cavity, at the antinode of the electromagnetic field. The DBR cavity can be seen as a 1-D photonic crystal in

Manuscript received July 19, 2001. The work of M. Pelton was supported by the Stanford Graduate Fellowships program. The work of G. S. Solomon was supported by the Army Research Office. The work of J. Vučković and A. Scherer was supported in part by the Caltech MURI Center for Quantum Networks under ARO Grant DAAD19-00-1-0374.

M. Pelton is with the Quantum Entanglement Project, ICORP, E.L. Ginzton Laboratory, Stanford University, Stanford, CA 94305 USA.

J. Vučković and A. Scherer are with the Department of Electrical Engineering, California Institute of Technology, Pasadena, CA 91125 USA.

G. S. Solomon is with the Quantum Entanglement Project, ICORP, E.L. Ginzton Laboratory, Stanford University, Stanford, Stanford, CA 94305 USA and also with the Solid-State Photonics Laboratory, Stanford University, Stanford, CA 94305 USA.

Y. Yamamoto is with the Quantum Entanglement Project, ICORP, E.L. Ginzton Laboratory, Stanford University, Stanford, CA 94305 USA and also with NTT Basic Research Laboratories, Atsugishi, Kanagawa, Japan

Publisher Item Identifier S 0018-9197(02)00626-7.

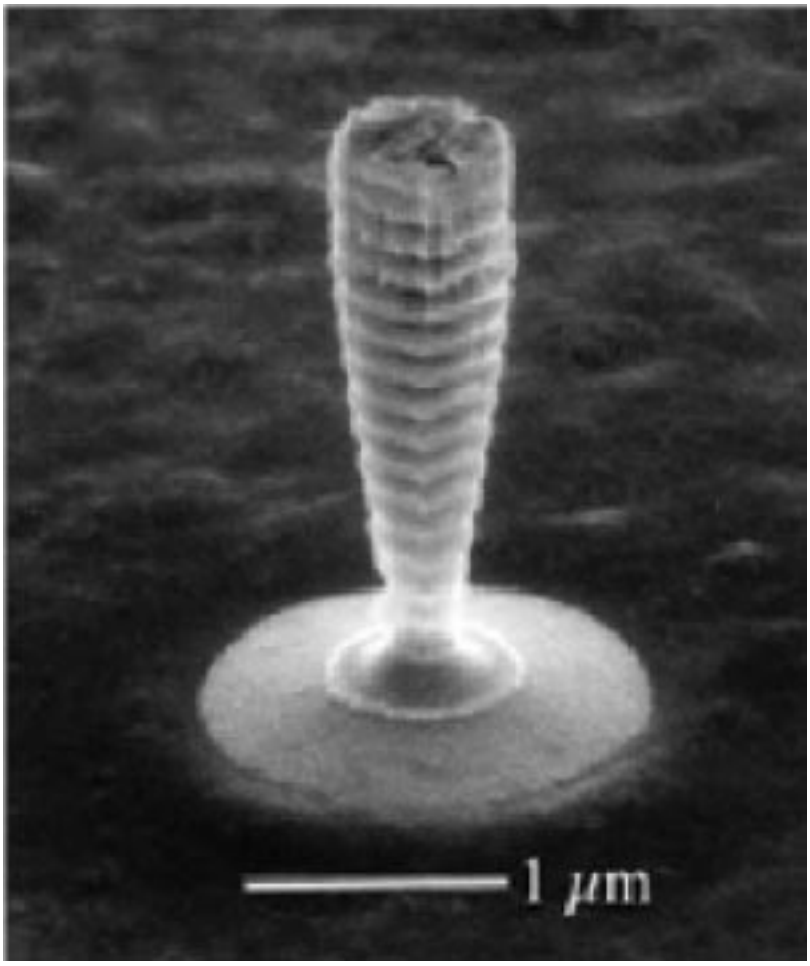

Fig. 1. Scanning-electron microscope image of a micropost microcavity. The diameter at the top of the post is 0.5 μm.

a waveguide, with the spacer layer acting as a crystal defect. In this sense, the cavity modes are analogous to defect modes in other 1-D photonic crystals [16].

The structure is fabricated as follows. Planar DBR mirrors are deposited epitaxially on a GaAs wafer by molecular-beam epitaxy (MBE), which allows for precise control over layer thickness. The spacer layer is grown with a taper, so that the cavity resonant wavelength varies across the wafer. A layer of InAs quantum dots is grown in the center of the spacer layer during the same MBE deposition. Epitaxy of InAs on GaAs leads to the formation of defect-free nanometer-scale islands, which form spontaneously after the deposition of a planar wetting layer in order to relieve strain [17]–[19]. Carriers are trapped in the islands because of the bandgap difference between the two materials. Due to the small size of the dots, only discrete energy levels are allowed, which, in turn, means that optical transitions occur only at discrete wavelengths. The dots are grown at a relatively low density of about 75 μm^{-2}, so that they can be easily isolated.

Following the MBE growth, a metal mask is deposited on the sample surface using electron-beam lithography followed by a liftoff process. The sample is then etched in an electron-cyclotron resonance (ECR) plasma etcher. In this process, a low-temperature, low-density mixture of argon, chlorine, and boron trichloride gases is ionized by microwaves at the ECR frequency. The resulting plasma is magnetically confined above the sample, and ions are accelerated toward the sample by an applied radio-frequency field. This gives an anisotropic etch, allowing high-aspect-ratio structures to be formed. However, an unavoidable by-product of the etch is undercutting of the posts, as can be seen in Fig. 1. We believe that this undercut is the result of sample heating by ion bombardment during the etch. When calculating mode structure, it is important to consider the tapered shape of the posts. Also important is the fact that the etch in these structures extends only through the top DBR stack, the spacer layer, and part of the lower stack.

III. FDTD Model

The only way to accurately model optical modes in such a complex structure as described above is to numerically solve Maxwell's equations. One of the most popular ways of doing so is the FDTD method, proposed by Yee in 1966 [20]. This method is based on a discretization of the differential form of Maxwell's equations. More explicitly, the following two Maxwell's equations are solved numerically:

$$\mu_o \frac{\partial \mathbf{H}}{\partial t} = -\nabla \times \mathbf{E}$$
$$\epsilon \frac{\partial \mathbf{E}}{\partial t} = \nabla \times \mathbf{H} \tag{1}$$

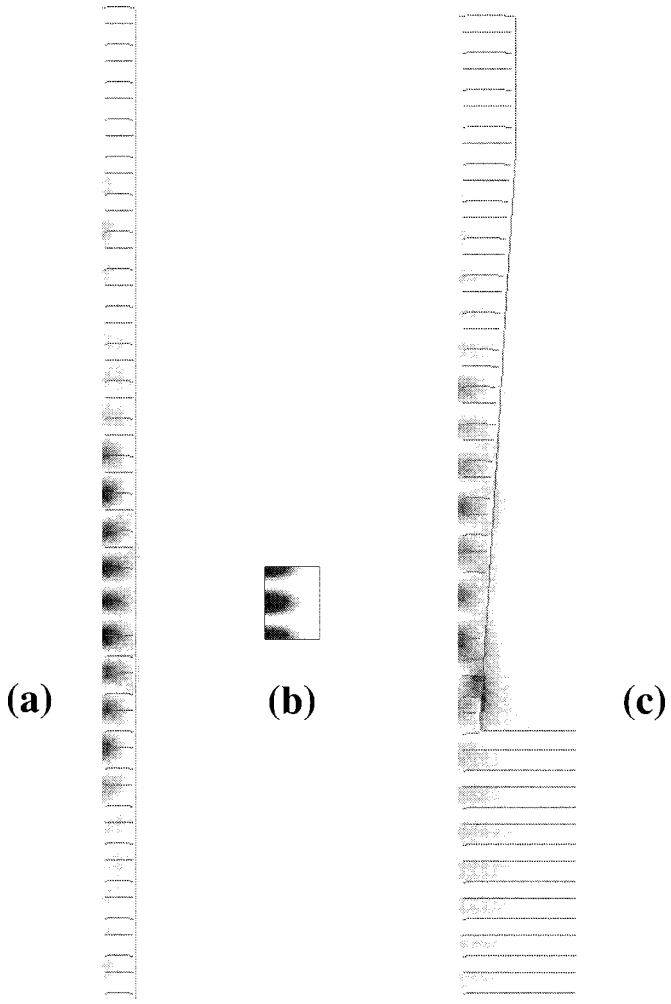

Fig. 2. Electric field intensity for the fundamental mode of a micropost microcavity with a top diameter of 0.5 μm. The intensity is represented by grayscale shading. Half a longitudinal cross-section of the post is shown. The 3-D intensity distribution can be obtained by rotating around an axis running down the center of the post (left-hand side of the figures). Lines represent interfaces between different materials. The field in (a) is calculated by the FDTD method for an ideal post, where the sidewalls are straight and the etch extends completely through the lower mirror. (b) Corresponding field near the center of the post calculated by the approximate method. (c) Field calculated by the FDTD method for realistic posts, where the sidewalls are tapered and the etch only extends partially through the lower mirror.

where $\mathbf{E}$ and $\mathbf{H}$ are the electric and magnetic fields, respectively, and ϵ is the dielectric constant of the medium. A Cartesian spatial grid is defined with increments Δx, Δy, and Δz, and a time increment Δt is also defined. Any field $F(x,y,z,t)$ can then be written in discretized form as $F^n(i,j,k) = F(i\Delta x, j\Delta y, k\Delta z, n\Delta t)$. The electric and magnetic fields are defined on two grids that are offset by half a step in time and space. The fields can then be alternately advanced in time, using a leapfrog method. Six coupled finite-difference equations are solved, one for each of the components of the electromagnetic fields. For example, the z-component of the electric field is given by (2), shown at the bottom of the page. The computational mesh is truncated by placing a nonreflecting absorber at all boundaries [21].

We use this method to determine the modes of a micropost microcavity. An initial field distribution is applied to the analyzed structure, and the fields are subsequently evolved in time. We record the time evolution of the field at a point of low symmetry, and take the fast Fourier transform of the resulting time series to get the cavity mode spectrum. We then identify a mode of interest with frequency ω_o. The mode is isolated by convolving the field in time (at each point of the computational domain) with an oscillating function of frequency ω_o. In the frequency domain, this convolution corresponds to the application of a band-pass filter with central frequency ω_o and with a linewidth determined by the boundaries of the convolution integral. We ignore mode polarization in this analysis, so that any pair of polarization-degenerate modes will be treated as one mode.

We can take advantage of the rotational symmetry of the cavities to make the calculations more efficient, reducing the order of the computer memory requirements from N^3 to N^2, where N represents a linear dimension of the computational domain [22]. In this case, each simulation performed by the cylindrical FDTD algorithm is for a particular value of the azimuthal mode number m.

The flexibility of the FDTD method allows simulation of both ideal structures with straight walls and realistic structures with posts that are undercut as a result of etching. We take the refractive indices of GaAs and AlAs to be 3.57 and 2.94, respectively, and the thicknesses of GaAs and AlAs mirror layers to be 70 and 85 nm, respectively. The central GaAs spacer layer is 280-nm thick and is sandwiched between 15 mirror pairs on top and 30 mirror pairs on bottom. The entire structure rests on a GaAs substrate. Absorption losses are neglected. The spatial discretization is performed with a 5-nm mesh. For ideal structures, we assume straight walls and etching through the entire bottom mirror. For tapered structures, the etch extends through only the top two pairs of the bottom mirror. Also, in these realistic posts, the cavity diameter is constant for only 550 nm on top, after which it changes linearly with a slope of approximately 4° with respect to the micropost axis.

Fig. 2 shows the calculated electric field intensity of the lowest order mode in structures with a cavity diameter of 0.5 μm at the top of the post. Fig. 2(a) shows an ideal post, while

$$E_z^{n+1}\left(i,j,k+\frac{1}{2}\right) = E_z^n\left(i,j,k+\frac{1}{2}\right) + \frac{\Delta t}{\epsilon\left(i,j,k+\frac{1}{2}\right)} \cdot \left[\frac{H_y^{n+\frac{1}{2}}\left(i+\frac{1}{2},j,k+\frac{1}{2}\right) - H_y^{n+\frac{1}{2}}\left(i-\frac{1}{2},j,k+\frac{1}{2}\right)}{\Delta x} - \frac{H_x^{n+\frac{1}{2}}\left(i+\frac{1}{2},j,k+\frac{1}{2}\right) - H_x^{n+\frac{1}{2}}\left(i,j-\frac{1}{2},k+\frac{1}{2}\right)}{\Delta y}\right]. \quad (2)$$

TABLE I
QUALITY FACTOR Q AND RESONANCE WAVELENGTH λ FOR THE FUNDAMENTAL MODES OF IDEAL AND REALISTIC MICROPOST MICROCAVITIES, AS CALCULATED BY THE FDTD METHOD

Diameter (μm)	Ideal Q	Ideal λ (nm)	Realistic Q	Realistic λ (nm)
0.5	5000	920	166	915
1.0	7000	976	440	962
2.0	11 500	993	2500	992
∞	12 000	1000	–	–

Fig. 2(c) shows a realistic post. A significant difference in the field distribution can be seen between the two posts.

The quality factor of a mode is determined by two independent methods: 1) the decay time constant for energy stored in the mode and 2) the ratio of the energy stored in the cavity, multiplied by the mode frequency, to the power lost by radiation outside the cavity. Table I lists the values of Q calculated for the fundamental modes of ideal posts with three different diameters. It can be seen that the quality factor decreases as the posts get smaller. This is due to the blue shift in the fundamental mode, also indicated in Table I. As the post diameter decreases, the mode becomes more tightly confined, and its wavelength decreases. The resonance wavelength is, thus, no longer the wavelength for which the DBRs were designed. At the same time, the effective incident angle of light on the DBRs increases. Both these effects cause the effective mirror reflectivity to decrease slightly.

A much more dramatic decrease in quality factor is seen when we consider posts of realistic shape, as indicated in Table I and Fig. 3. As can also be seen, the blue shift is similar to that for ideal posts; the wavelength shift thus cannot account for the degradation of Q. The additional loss in these posts is due to diffraction in the lower DBR. Light making a longitudinal round-trip in the cavity penetrates a certain distance into the unetched portion of the lower DBR before being reflected back. As it does so, it diffracts outwards, so that only a certain fraction of the light is recaptured in the post. This is also manifested in the significant field intensity outside of the lower portion of the realistic post in Fig. 2(c)

The analysis of Purcell factors is based on a method presented in [23]. The total radiated power is calculated for a classical dipole in the cavity and for a dipole in bulk material. The ratio of these powers gives the Purcell factor. Fig. 4(a) shows the Purcell factors calculated for single quantum dots on resonance with the fundamental mode of cavities with realistic shapes. The quantum dots are assumed to be located near the center of the posts. The degradation in Q is seen to overtake the reduction in mode volume, reducing the Purcell factor as the post diameter decreases. Nonetheless, significant enhancement of spontaneous emission rate is seen for posts of all sizes.

IV. APPROXIMATE MODEL

The FDTD calculations are demanding in terms of computer resources and processing time. We, therefore, developed an approximate, heuristic model, in an attempt to reproduce the major results in a simpler fashion. We followed Panzarini and Andreani [24] and assumed that the field distribution can be separated into two parts, one that depends only on the transverse coordinates r and θ, and one that depends only on the longitudinal coordinate z; i.e., $E(r,\theta,z) = E_r(r,\theta)E_z(z)$.

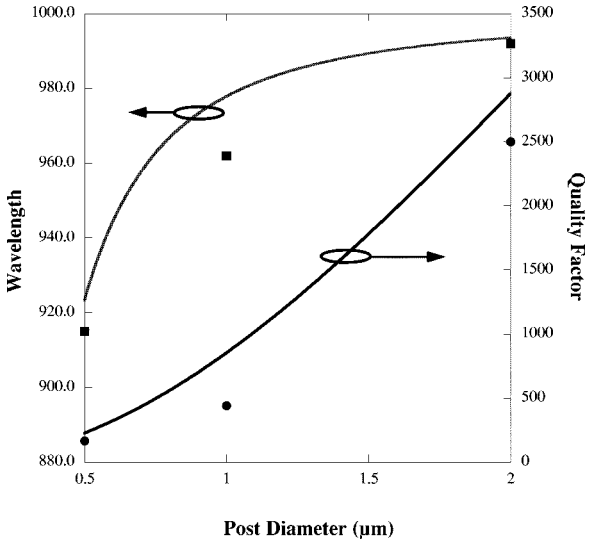

Fig. 3. Quality factor and resonance wavelength for the fundamental modes of realistic micropost microcavities. Points indicate values calculated by the FDTD method, and solid lines indicate values calculated by the approximate method.

The longitudinal field dependence is calculated using a standard transfer-matrix method [25]. We consider a plane wave incident on a planar structure in the normal direction. The foward- and backward-propragating amplitudes at any point constitute a two-component vector. The field vector $\mathbf{v}'$ after the boundary can be determined from the field vector $\mathbf{v}$ before the boundary by multiplying by the appropriate transfer matrix: $\mathbf{v}' = \mathbf{M}\mathbf{v}$, where

$$\mathbf{M} = \frac{1}{2}\begin{bmatrix} 1+\frac{k_2}{k_1} & 1-\frac{k_2}{k_1} \\ 1-\frac{k_2}{k_1} & 1+\frac{k_2}{k_1} \end{bmatrix}. \tag{3}$$

In this matrix, k_1 and k_2 are the wavenumbers before and after the boundary, respectively. Propagation through a uniform layer of thickness l is likewise described by a transfer matrix

$$\mathbf{M} = \begin{bmatrix} e^{ikl} & 0 \\ 0 & e^{-ikl} \end{bmatrix}. \tag{4}$$

The product of successive matrices $\mathbf{M_n M_{n-1} \ldots M_2 M_1}$ gives the relation between the fields at any two points in the structure. The field distribution in the longitudinal direction can thus be calculated. It has a maximum in the center of the spacer layer, and decays over an effective penetration depth l_{eff} in the DBR's. An effective refractive index n_{eff} can be calculated by taking an average of the material indices across the planar structure, weighted point by point by the electric field intensity.

The field in the transverse direction is then determined by considering an infinitely long, cylindrical, dielectric waveguide with refractive index n_{eff}. Modes of this waveguide can be determined by the usual application of boundary conditions [26]. This results in a characteristic equation with multiple solutions

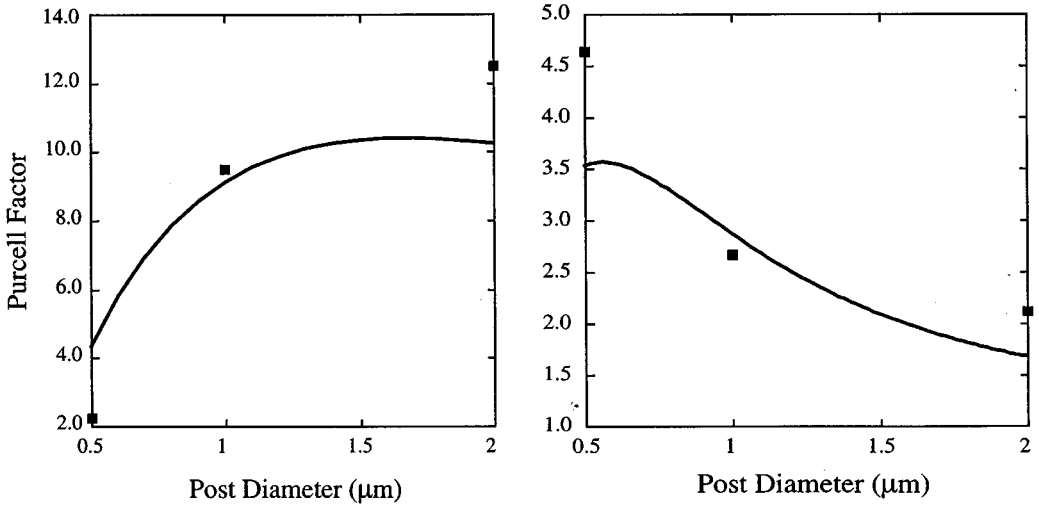

(a) (b)

Fig. 4. Purcell factors for quantum dots resonant with the fundamental modes of realistic micropost microcavities. The Purcell factor is the ratio of the spontaneous emission rate for a dot resonant with the cavity mode to the spontaneous emission rate in the absence of the cavity. (a) Calculated results for a single dot at the center of the post. The points are values calculated by the finite-difference time-domain method, and the line is calculated by the approximate method. (b) Compares experimentally measured values (points) with the average values calculated by the approximate method for a large number of dots distributed radially across the post (line).

in general, each one corresponding to a waveguide mode. The boundary conditions also give the field distribution in the plane. For example, the fundamental HE_{11} mode has the following transverse electric field profile:

$$\mathbf{E_t}(r,\theta) \propto \left\{ \begin{array}{c} J_0(\beta r) \\ K_0(\beta r) \end{array} \right\} (\hat{\mathbf{x}} - i\hat{\mathbf{y}}) \tag{5}$$

where J_0 and K_0 are zeroth-order Bessel functions of the first and second kind, respectively, and the transverse wavenumber β is obtained from the characteristic equation. In this equation, the top line refers to fields inside the waveguide, and the bottom line to fields outside the waveguide. The overall wavenumber k can be obtained by assuming that the longitudinal wavenumber is unchanged from the unguided value k_o: $k \approx \sqrt{k_o^2 + \beta^2}$. This allows, for example, the resonance wavelength of the HE_{11} mode to be determined, as shown in Fig. 3. The blueshift with decreasing post diameter is seen to be similar to that calculated by the FDTD method.

Once the longitudinal and transverse fields have been calculated, they are multiplied together point by point to give the 3-D field distribution. Fig. 2(b) shows the field intensity calculated for the fundamental mode near the center of a post with a diameter of 0.5 μm. The distribution is quite similar to the results of the FDTD calculations for the ideal post. In addition, the Bessel function describing the transverse field dependence is well approximated by a Gaussian, meaning that light that escapes through the top of the post is emitted in a Gaussian-like traveling wave. This allows for efficient couping to optical fibers and other downstream elements.

This model, though, treats the post as a quasiinfinite waveguide, and thus does not account for diffraction loss in the lower DBR. The loss must added to the model heuristically. A wave with an initial transverse profile given by the waveguide mode is allowed to propagate freely for twice the DBR penetration depth l_{eff}. This represents spreading of the field as it penetrates into the unetched lower mirror and is reflected back to the post. The overlap integral between the propagated field and the waveguide mode is then calculated, giving the fraction of the wave that is recaptured by the post. The remainder is taken to be an additional reflection loss in the lower DBR. Although this theory is approximate, it reproduces well the modal quality factors determined by the FDTD method, as seen in Fig. 3. This lends support to our interpretation of the mechanism for degradation of Q in realistic posts.

Once the field distribution and quality factor have been calculated, the Purcell factor can be determined, according to the following formula:

$$\frac{\gamma}{\gamma_0} = \frac{Q\lambda^3}{2\pi^2 n_{eff}^3 V_0} + f \tag{6}$$

where λ is the cavity resonant wavelength, and we have assumed zero detuning between the quantum dot emission and the cavity resonance. The mode volume V_o is calculated by integrating the field intensity over space and normalizing by the peak intensity. The decay rate into leaky modes is $f\gamma_o$. Loss into unguided modes is taken to consist of two parts: light incident on the DBRs at an angle greater than the limit of the angular stopband, and light incident on the post edges at an angle less than the critical angle for total internal reflection. For posts with small diameters, only the second factor contributes; in this case, f is constant at about 0.3.

Purcell factors calculated by this method are shown in Fig. 4(a). General agreement with the FDTD results is seen. This means that the heuristic model gives a relatively simple method for estimating the coupling between quantum dots and modes of realistic micropost microcavities.

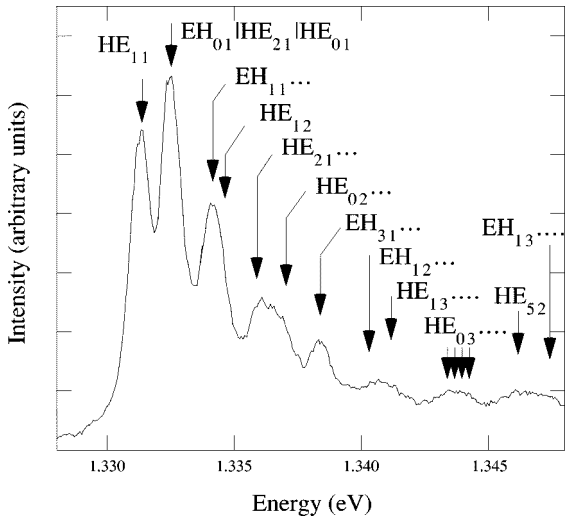

Fig. 5. Photoluminescence from a micropost microcavity with diameter 6 μm, which contains a large number of quantum dots. The cavity modes are labeled according to the transverse waveguide modes in the approximate theory. The arrows are at the calculated resonance wavelengths.

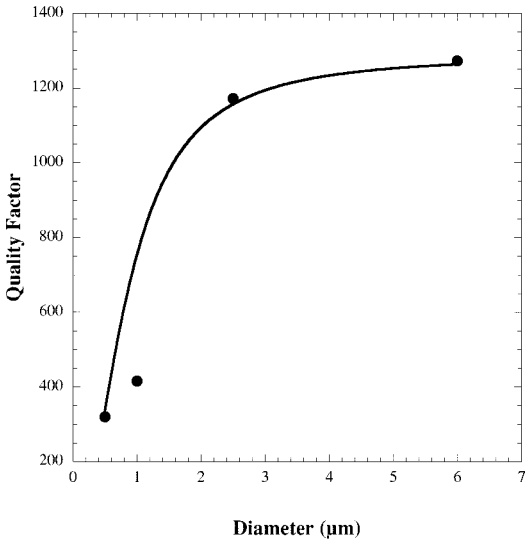

Fig. 6. Quality factor of the fundamental modes of micropost microcavities. Points indicate experimentally measured values, and solid lines indicate values calculated by the approximate method, including additional reflection loss in the distributed-Bragg mirrors.

V. Comparison of Models to Experimental Results

Finally, we would like to test our models by comparing their predictions to experimental results [11]. We fabricated micropost microcavities containing quantum dots, as described in Section II. The sample was held near a temperature of 4 K in a continuous-flow liquid-helium cryostat. Electron-hole pairs were created in the GaAs matrix surrounding the dots by excitation with pulses from a mode-locked Ti:sapphire laser. The carriers are trapped in the dots and relax to the ground state, where they recombine radiatively. The emitted light is analyzed by a spectrometer.

Larger posts contain many dots with varying sizes and shapes. The luminescence is thus inhomogeneously broadened over a large energy range. This broadband emission is filtered by the cavity modes, so that several narrower lines are observed in the radiation from the posts. The quality factor of the modes can be determined from the linewidths of these resonances. A sample spectrum from a post with diameter of 6 μm is shown in Fig. 5. The arrows indicate resonance wavelengths calculated by the approximate method, labeled according to the transverse waveguide modes.

Smaller posts, on the other hand, contain only a small number of dots, and luminescence occurs only in narrow, discrete quantum-dot lines. For high excitation power, however, these quantum-dot lines are accompanied by a weaker broadband fluorescence. The origin of this continuum luminescence is unclear; one possibility is that it results from partially localized states in the wetting layer [27]. Regardless of its source, the broadband emission is filtered by the cavity mode, allowing a measurement of cavity linewidth.

The quality factors as determined from the measured linewidths are plotted in Fig. 6. The values for posts with larger diameters are seen to be lower than those in Fig. 3. This is partially due to imperfections in the MBE-grown DBR mirrors, including roughness at the AlAs/GaAs interfaces and deviations between designed and actual layer thicknesses. It is also due to the taper in the cavity spacer layer. The nonideal DBRs are accounted for phenomenologically in the approximate theory by introducing additional reflection losses in the top and bottom DBRs. The magnitude of these losses is set to match the independently measured Q of 2300 for the planar cavity. The results of the approximate theory with this additional loss factor are also shown in Fig. 6, and are seen to agree well with experimental results. Note that the FDTD method predicts the experimentally observed Q for posts with diameters of 0.5 μm, where the diffraction loss dominates over imperfections in the DBRs. This indicates that, in practice, quality factors of small posts are limited by diffraction losses, and not by other phenomena such as sidewall scattering or imperfect DBRs.

For measurements of recombination rate, the emitted light is sent through a spectrometer to a streak camera, giving time- and frequency-resolved luminescence intensities. The time traces are integrated over a narrow window around the resonance frequency, and an exponential is fitted to the latter part of each of the resulting curves. The time constants of these exponentials gives the radiative lifetimes of quantum dots in the posts. By comparing to the independently-measured lifetime of 1.3 ns for quantum dots without microcavities, the Purcell factor can be obtained. The measured Purcell factors are shown in Fig. 4(b). For post diameters larger than 0.5 μm, the measured Purcell factors are smaller than the theoretical values plotted in Fig. 4(a). In these posts, several dots are resonant with the cavity mode, and their radial location in the dot is unknown. Rather than considering a single dot on resonance with the post, then, we must average the Purcell factor for different radial locations of the dot. This is added to the approximate theory, and the results are shown in Fig. 4(b). Good agreement with experimental data is seen. It is worth noting that the radially-averaged Purcell factor reaches a maximum at a post diameter of about 0.6 μm, unlike the Purcell factor for a single dot at the center of the post, which decreases monotonically with post diameter.

VI. Conclusion

We have used finite-difference time-domain simulations to model the optical mode characteristics of ideal and realistic micropost microcavities. We are able to accurately predict quality factors of modes in posts, as well as modification of spontaneous-emission lifetime of single quantum dots inside the microcavities. An approximate theory has been developed, which reproduces the main features of the FDTD model and of experimental results. This allows us to say with confidence that micropost microcavities are a good system for achieving significant coupling between discrete optical modes and quantum-dot excitons. In all cases, agreement between theory and experiment is obtained with no fitting parameters. The theories can thus immediately be extended to structures with different shapes and compositions.

The calculations have also demonstrated that the limitation in coupling single quantum dots to modes of micropost microcavities has been the shape of the posts, which results in diffraction loss in the lower mirror. By improving the semiconductor process used to make the microposts, it should be possible to approach ideal, straight-walled posts that extend completely through the lower DBR stack. This will give greater lifetime modification: FDTD calculations predict a Purcell factor of as much as 147 for ideal posts with a diameter of 0.5 μm. Optimization of the design of the micropost microcavities should improve the quality factor and increase the coupling to quantum dots even further, allowing new physical phenomena to be observed.

Acknowledgment

The authors thank H. Deng for valuable assistance.

References

[1] E. M. Purcell, "Spontaneous emission probabilities at radio frequencies," *Phys. Rev.*, vol. 69, p. 681, 1946.
[2] K. H. Drexhage, *Progress in Optics*. Amsterdam, The Netherlands: North-Holland, 1974, vol. XII, pp. 165–232.
[3] P. Goy, J.-M. Raimond, M. Gross, and S. Haroche, "Observation of cavity-enhanced single-atom spontaneous emission," *Phys. Rev. Lett.*, vol. 50, pp. 1903–1906, 1983.
[4] G. Gabrielse and H. Dehmelt, "Observation of inhibited spontaneous emission," *Phys. Rev. Lett.*, vol. 55, pp. 67–70, 1985.
[5] R. G. Hulet, E. S. Hilfer, and D. Kleppner, "Inhibited spontaneous emission by a Rydberg atom," *Phys. Rev. Lett*, vol. 55, pp. 2137–2140, 1985.
[6] B. Gayral, J. M. Gérard, A. Lematre, C. Dupuis, L. Manin, and J. L. Pelouard, "High-Q wet-etched GaAs microdisks containing InAs quantum boxes," *Appl. Phys. Lett.*, vol. 75, pp. 1908–1910, 1999.
[7] C. J. M. Smith, H. Benisty, D. Labilloy, U. Oesterle, R. Houdre, T. F. Krauss, R. M. De La Rue, and C. Weisbuch, "Near-infrared microcavities confined by two-dimensional photonic bandgap crystals," *Electron. Lett.*, vol. 35, pp. 228–230, 1999.
[8] B. Ohnesorge, M. Bayer, A. Forchel, J. P. Reithmaier, N. A. Gippius, and S. G. Tikhodeev, "Enhancement of spontaneous emission rates by three-dimensional photon confinement in Bragg microcavities," *Phys. Rev. B*, vol. 56, pp. R4367–4370, 1997.
[9] J. M. Gérard, B. Sermage, B. Gayral, B. Legrand, E. Costard, and V. Thierry-Mieg, "Enhanced spontaneous emission by quantum boxes in a monolithic optical microcavity," *Phys. Rev. Lett.*, vol. 81, pp. 1110–1113, 1998.
[10] L. A. Graham, D. L. Huffaker, and D. G. Deppe, "Spontaneous lifetime control in a native-oxide-apertured microcavity," *Appl. Phys. Lett*, vol. 74, pp. 2408–2410, 1999.
[11] G. S. Solomon, M. Pelton, and Y. Yamamoto, "Single-mode spontaneous emission from a single quantum dot in a three-dimensional microcavity," *Phys. Rev. Lett.*, vol. 86, pp. 3903–3906, 2001.
[12] P. Michler, A. Kiraz, C. Becher, W. V. Schoenfeld, P. M. Petroff, L. Zhang, E. Hu, and A. Imamoglu, "A quantum dot single-photon turnstile device," *Science*, vol. 290, pp. 2282–2285, 2000.
[13] C. Santori, M. Pelton, G. S. Solomon, Y. Dale, and Y. Yamamoto, "Triggered single photons from a quantum dot," *Phys. Rev. Lett*, vol. 86, pp. 1502–1505, 2001.
[14] T. Baba, T. Hamano, F. Koyama, and K. Iga, "Spontaneous emission factor of a microcavity DBR surface-emitting laser," *IEEE J. Quantum Electron.*, vol. 27, pp. 1347–1358, 1991.
[15] ——, "Spontaneous emission factor of a microcavity DBR surface emitting laser. II. Effects of electron quantum confinements," *IEEE J. Quantum Electron.*, vol. 28, pp. 1310–1319, 1992.
[16] J. S. Foresi, P. R. Villeneuve, J. Ferrera, E. R. Thoen, G. Steinmeyer, S. Fan, J. D. Joannopoulos, L. C. Kimerling, H. I. Smith, and E. P. Ippen, "Photonic-bandgap microcavities in optical waveguides," *Nature*, vol. 390, pp. 143–145, 1997.
[17] M. Tabuchi, S. Noda, and A. Sasaki, *Science and Technology of Mesoscopic Structures*. New York: Springer-Verlag, 1992, p. 375.
[18] D. Leonard, M. Krishnamurthy, C. M. Reaves, S. P. Denbaars, and P. M. Petroff, "Direct formation of quantum-sized dots from uniform coherent islands of InGaAs on GaAs surfaces," *Appl. Phys. Lett*, vol. 63, pp. 3203–3205, 1993.
[19] J. Y. Marzin, J. M. Gérard, A. Izraël, D. Barrier, and G. Bastard, "Photoluminescence of single InAs quantum dots obtained by self-organized growth on GaAs," *Phys. Rev. Lett*, vol. 73, pp. 716–719, 1994.
[20] K. S. Yee, "Numerical solution to initial boundary value problems involving maxwell's equations in isotropic media," *IEEE Trans. Antennas Propagat.*, vol. AP-14, pp. 302–307, 1966.
[21] A. Taflove, *Computational Electrodynamics: The Finite-Difference Time-Domain Method*. Norwood, MA: Artech, 1995.
[22] Y. Chen, R. Mittra, and P. Harms, "Finite-difference time-domain algorithhm for solving Maxwell's equations in rotationally symmetric geometries," *IEEE Trans. Microwave Theory Tech.*, vol. 44, pp. 832–838, 1996.
[23] Y. Xu, J. Vučković, R. Lee, O. Painter, A. Scherer, and A. Yariv, "Finite-difference time-domain calculation of spontaneous emission lifetime in a microcavity," *J. Opt. Soc. Amer. B*, vol. 16, pp. 465–474, 1999.
[24] G. Panzarini and L. C. Andreani, "Quantum theory of exciton polaritons in cylindrical semiconductor microcavities," *Phys. Rev. B*, vol. 60, pp. 16 799–16 806, 1999.
[25] G. Björk, H. Heitmann, and Y. Yamamoto, "Spontaneous-emission coupling factor and mode characteristics of planar dielectric microcavity lasers," *Phys. Rev. A*, vol. 47, pp. 4451–4463, 1993.
[26] A. W. Snyder and J. D. Love, *Optical Waveguide Theory*. London, U.K.: Chapman & Hall, 1983.
[27] Y. Toda, O. Moriwaki, M. Nishioka, and Y. Arakawa, "Efficient carrier relaxation mechanism in InGaAs/GaAs self-assembled quantum dots based on the existence of continuum states," *Phys. Rev. Lett.*, vol. 82, pp. 4114–4117, 1999.

Matthew Pelton recieved the B.A.Sc. degree in engineering science from the University of Toronto, Toronto, Canada, in 1996. He is currently working toward the Ph.D. degree at Stanford University, Stanford, CA.

Since 1996, he has been a Research Assistant in the Applied Physics Department of Stanford University. His current research interests include cavity quantum electrodynamics with single quantum dots, and single-dot devices, including single-photon emitters.

Jelena Vučković (M'01) received the Dipl. Ing. degree from the Faculty of Electronic Engineering, University of Nis, Nis, Yugoslavia, in 1993, the M.S. degree in electrical engineering in June 1997, and the Ph.D. degree in electrical engineering in 2001, both from the CalTech Nanofabrication Group, California Institute of Technology, Pasadena.

During 1994 and 1995, she was a Research Associate in the Microcomputer Systems Group at the University of Nis, and in 1996, a Researcher in the Communications Science and Engineering Group, School of Electrical Engineering, the University of Sydney, Sydney, Australia. In September 1996, she joined the CalTech Nanofabrication Group. Her research interests include photonic-crystal-based optical devices, computational electromagnetics, and nanofabrication techniques.

Glenn S. Solomon received the B.S.E. and M.S.E. degrees in mechanical engineering and materials science from Duke University, Durham, NC, in 1980 and 1983, respectively, the M.S.E. degree in electrical engineering in 1995, and the Ph.D. degree in materials science and engineering in 1997, both from Stanford University, Stanford, CA, .

From 1983 to 1989, he was a Research Engineer for Research Triangle Institute, NC. From 1996 to 1998, he was a Research Associate with Ginzton Laboratories, Stanford University. He has been President and CEO of CBL Technologies, Redwood City, CA, since 1997. Since 1999, he has been an Acting Assistant Professor in the Department of Electrical Engineering, Stanford University. His current research interests include self-assembled quantum dots, cavity quantum electrodynamics, nitride materials development, and spin-based electronic devices.

Axel Scherer received the B.S., M.S., and Ph.D. degrees from the New Mexico Institute of Mining and Technology, Socorro, in 1981, 1982, and 1985, respectively.

From 1985 to 1993, he was with the Quantum Device Fabrication Group at Bellcore. Currently, he is the Neches Professor of Electrical Engineering, Applied Physics and Physics at California Institute of Technology, Pasadena, CA, and a leader of the CalTech Nanofabrication Group. His research interests include design and fabrication of functional photonic, nanomagnetic, and microfluidic devices.

Yoshihisa Yamamoto (S'75–M'84–SM'91) received the Ph.D. degree from the University of Tokyo, Tokyo, Japan, in 1978.

He joined NTT Basic Research Laboratories, Kanagawa, Japan, the same year, where he served as the leader of the Yamamoto Research Group from 1987 to 1992. In 1992, he joined Stanford University, Stanford, CA, as a Professor of Applied Physics and Electrical Engineering, while continuing to serve as a Research Fellow at NTT. From 1993 to 1998, he was the Director of the Yamamoto Quantum Fluctuation Project, ERATO, Yamamoto, Japan. In 1999, he was appointed co-leader of the ERATO Quantum Fluctuation Project at Stanford University, Stanford, CA. His current research interests are in the areas of quantum optics, mesoscopic physics, and quantum information technologies.